
HoSNNs: Adversarially-Robust Homeostatic Spiking Neural Networks with Adaptive Firing Thresholds

Hejia Geng

University of California, Santa Barbara
Santa Barbara, CA 93106
hejia@ucsb.edu

Peng Li

University of California, Santa Barbara
Santa Barbara, CA 93106
lip@ucsb.edu

Abstract

While spiking neural networks (SNNs) offer a promising neurally-inspired model of computation, they are vulnerable to adversarial attacks. We present the first study that draws inspiration from neural homeostasis to design a threshold-adapting leaky integrate-and-fire (TA-LIF) neuron model and utilize TA-LIF neurons to construct the adversarially robust homeostatic SNNs (HoSNNs) for improved robustness. The TA-LIF model incorporates a self-stabilizing dynamic thresholding mechanism, offering a local feedback control solution to the minimization of each neuron’s membrane potential error caused by adversarial disturbance. Theoretical analysis demonstrates favorable dynamic properties of TA-LIF neurons in terms of the bounded-input bounded-output stability and suppressed time growth of membrane potential error, underscoring their superior robustness compared with the standard LIF neurons. When trained with weak FGSM attacks ($\epsilon = 2/255$) and tested with much stronger PGD attacks ($\epsilon = 8/255$), our HoSNNs significantly improve model accuracy on several datasets: from 30.54% to 74.91% on FashionMNIST, from 0.44% to 35.06% on SVHN, from 0.56% to 42.63% on CIFAR10, from 0.04% to 16.66% on CIFAR100, over the conventional LIF-based SNNs.

1 Introduction

While neural network models have gained widespread adoption across many domains, a glaring limitation of these models has also surfaced — vulnerability to adversarial attacks [56, 36]. Subtle alterations in the input can trick a well-tuned neural network to produce misleading predictions, particularly for mission critical applications [11]. This vulnerability is shared by both artificial neural networks (ANNs) and spiking neural networks (SNNs) [52, 53, 15], and stands in stark contrast to the inherent robustness of biological nervous systems, prompting interesting questions: Why is the human brain immune to such adversarial noise? Can we leverage biological principles to bolster the resilience of artificial networks?

Motivated by these questions, we offer a new perspective that connects adversarial robustness with homeostatic mechanisms prevalent in living organisms. Homeostasis maintains essential regulatory variables within a life-sustaining range [7, 13, 47, 25], and is crucial for stabilizing neural activity [59], supporting neurodevelopment [37], and minimizing noisy information transfer [63, 39]. Although some studies have investigated homeostasis in SNNs, such as the generalized leaky-integrate-and-fire (GLIF) models [3, 5, 6, 57], no prior work has connected homeostasis with adversarial robustness.

We aim to close this gap by exploring an online biologically-plausible defense solution based on homeostasis. The proposed approach differs from common practices such as adversarial training in a major way, it explicitly builds a localized neural-level self-adapting feedback mechanism into the dynamic operation of the proposed HoSNNs. We view the time-evolving state, i.e., membrane potential $u_i(t|x)$ of each spiking neuron i in a well trained network as its representation of the

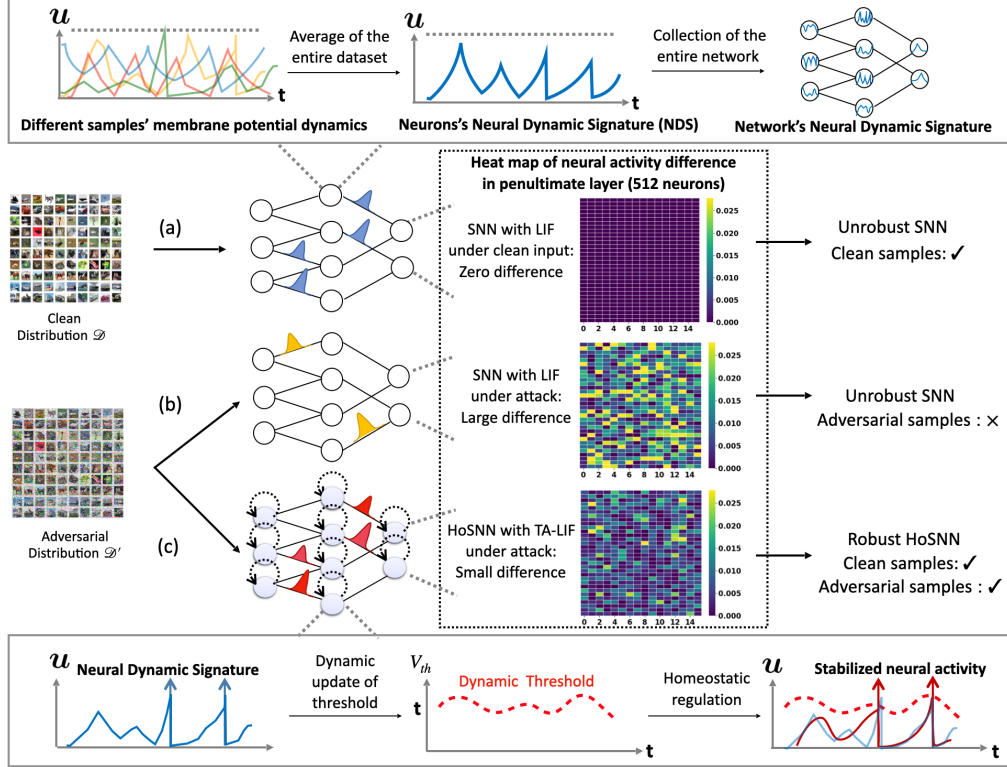


Figure 1: Proposed threshold-adapting leaky integrate-and-fire (TA-LIF) neuron model and homeostatic SNNs (HoSNNs). (a) We leverage a LIF SNN trained using clean data to collect neural dynamic signatures (NDS) as an anchor for the HoSNN (shown in the box above). (b) Adversarial inputs can cause large membrane potential deviations from the NDS in deep layers of LIF SNNs, leading to incorrect model predictions. (c) Homeostatic dynamic threshold voltage control in HoSNNs anchors neural activity based on the NDS, resulting improved robustness.

semantics of the received clean input x . Perturbed membrane potential $u_i(t|x')$ resulting from an adversarial input x' corresponds to distorted semantics and can ripple through successive layers to mislead the network output [32, 48, 42, 54, 17, 18, 26, 23]. For a given pair (x, x') , we ensure adversarial robustness by minimizing the total induced membrane potential perturbation $E_i(x, x')$.

We address two practical challenges encountered in formulating and solving this error minimization problem. Firstly, during inference the clean membrane potential $u_i(t|x)$ reference is unknown. As shown in Fig 1(a), we define Neural Dynamic Signature (NDS), the neuron’s membrane potential averaged over a given clean training dataset \mathcal{D} , to provide a reference for anchoring membrane potential. Secondly, since externally generated attacks are not known *a priori*, it is desirable to suppress the perturbation of each neuron’s membrane potential in an online manner as shown in Fig 1(b). For this, we propose a new threshold-adapting leaky integrate-and-fire (TA-LIF) model with a properly designed firing threshold voltage dynamics that serves as a homeostatic control to suppress undesirable membrane potential perturbations, as shown in Fig 1(c). We theoretically analyze the dynamic properties of TA-LIF neurons in terms of the bounded-input bounded-output stability and suppressed time growth of membrane potential error, underscoring their superior robustness compared with the standard LIF neurons.

We visualize the working of the proposed HoSNNs versus standard LIF-based SNNs in image classification using several CIFAR-10 images in Figure 2. While the adversarial images generated by the Projected Gradient Descent (PGD) [36] attack can completely mislead the attention of the LIF SNN, the proposed homeostasis helps the HoSNN focus on parts of the input image strongly correlated with the ground truth class label, leading to significantly improved adversarial robustness as demonstrated in detail in Section 4.

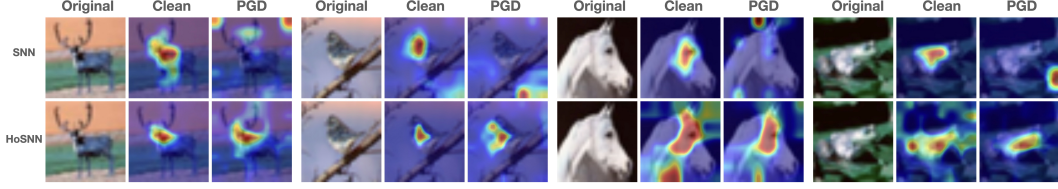


Figure 2: The heatmaps generated by Grad-CAM [51] highlight the regions of the input image that most significantly influence the classification decisions of a standard SNN and proposed HoSNN based on the VGG architecture for a set of CIFAR-10 images. The adversarial images are generated using PGD with an attack strength of $\epsilon = 6/255$. HoSNN can still maintain attention to the target object under attack. The original Grad-CAM method is adapted for SNNs, where each heatmap is computed with respect to the input image averaged across multiple time frames.

2 Background

2.1 Adversarial Attacks

Two notable adversarial attack techniques are the Fast Gradient Sign Method (FGSM) [22] and Projected Gradient Descent (PGD) [36] method. Let x be an original input, y be the true label, $L(\theta, x, y)$ the loss function with network parameters θ , and ϵ a small perturbation magnitude, FGSM generates a perturbed input, or an adversarial input example x' by: $x' = x + \epsilon \cdot \text{sign}[\nabla_x L(\theta, x, y)]$. PGD is essentially an iterative FGSM. With x_n as the perturbed input in the n -th iteration and α as the step size, $\text{Proj}_{x+\epsilon}\{\cdot\}$ as the projection within the ϵ -ball of x , PGD updates the input by: $x_{n+1} = \text{Proj}_{x+\epsilon}\{x_n + \alpha \cdot \text{sign}[\nabla_x L(\theta, x_n, y)]\}$. Other gradient-based attacks such as the RFGSM [58], Basic Iterative Method (BIM) [30], and DeepFool [40] work in a similar fashion. Beyond gradient-based methods [8], a significant area of concern is black-box attacks.

2.2 Defense Methods

Adversarial training is one of the most widely adopted defense methods [36], which retrains a model by using a mixture of clean and adversarial examples. Randomization [66] introduces stochasticity during inference and can circumvent precise adversarial attacks. The projection technique of [41] reverts adversarial attacks back to a safer set. Lastly, one may first detect the presence of adversarial attack and subsequently cope with it [38]. However, these defense methods are not free of limitations [2]. Adversarial training relies on precise gradient information and is not biologically plausible [35]. Randomization, projection, and detection strategies do not fundamentally address the inherent vulnerabilities of neural networks.

2.3 Spiking Neuron Models

SNNs allow for spike-based communication and computation [19, 20, 14] and often leverage the Leaky Integrate-and-Fire (LIF) model for each neuron i with the membrane time constant τ_m :

$$\tau_m \frac{du_i(t)}{dt} = -u_i(t) + I_i(t) - \tau_m s_i(t) V_{th}^i(t), \quad (1)$$

where $u_i(t)$ is the membrane potential, $I_i(t) \triangleq R \sum_j w_{ij} a_j(t)$ represents the input and is defined as the sum of the pre-synaptic currents; w_{ij} represents the synaptic weight from neuron j to i ; $V_{th}^i(t)$ is the firing threshold of neuron i at time t . Neuron i 's postsynaptic spike train is:

$$s_i(t) = \begin{cases} +\infty & \text{if } u_i(t) \geq V_{th}^i(t), \\ 0 & \text{otherwise} \end{cases} = \sum_f \delta(t - t_i^f) \quad (2)$$

where $\delta(\cdot)$ is the Dirac function, and t_i^f is a postsynaptic spike time. The LIF model uses a constant firing threshold. Generalized LIF (GLIF) models employ a tunable threshold with short-term memory, which increases with every emitted output spike, and subsequently decays exponentially back to the baseline threshold [3, 5, 6, 57]. However, these models neither consider adversarial robustness nor provides mechanisms to discern "abnormal" neural activity from "normal" activity.

2.4 Spiking Neural Networks Robustness

While there’s been growing interest in spiking neural networks [24, 46], empirical studies have demonstrated that SNNs exhibit similar susceptibilities to adversarial attacks [52, 15]. A line of research has explored porting defensive strategies developed for ANNs to SNNs. To improve the robustness of SNNs, [29] proposed a SNN training algorithm jointly optimizing firing thresholds and weights, and [34] proposed certified training. [15] enhanced adversarial training by using a Lipschitz constant regularizer. However, these methods have not fully addressed the challenges of ensuring adversarial robustness. Additionally, they are computationally expensive and lack biological plausibility. Another research direction has focused on studying the inherent robustness of SNNs not seen in their ANN counterparts, and factors impacting robustness. [53] recognized the inherent resistance of SNNs to gradient-based adversarial attacks. [16] investigated the impact of key network parameters such as firing voltage thresholds on robustness. [12] demonstrated the LIF model’s noise-filtering capability. [33] explored network inter-layer sparsity, and [67] examined the effects of surrogate gradient techniques on white-box attacks. While these studies have shed light on aspects of SNNs relevant to robustness, effective defense strategies are yet to be developed.

3 Method

We present the first study that draws inspiration from neural homeostasis to design a threshold-adapting leaky integrate-and-fire (TA-LIF) neuron model and utilize TA-LIF neurons to construct the adversarially robust homeostatic SNNs (HoSNNs) for improved robustness.

3.1 Adversarial Robustness as a Membrane Potential Error Minimization Problem

In a well trained network, we view the time-evolving state, i.e., membrane potential $u_i(t|x)$ of each spiking neuron i , over T timesteps as its representation of the semantics of the received clean input x . An adversarial input $x' = x + \epsilon\delta x$, where ϵ is the attack budget (strength), and δx is a carefully crafted adversarial noise, may lead to a perturbed membrane potential $u_i(t|x')$, which corresponds to distorted semantics and can ripple through successive layers to mislead the network’s decision [32, 48, 42, 54, 17, 18, 26, 23].

For a given pair of (x, x') , one may ensure adversarial robustness of the network by minimizing the total induced membrane potential perturbation $E_i(x, x')$ of all N neurons over T timesteps:

$$\min E_i(x, x') = \sum_{i=0}^N \sum_{t=0}^T \frac{1}{2} \| u_i(t|x') - u_i(t|x) \|^2 \quad (3)$$

However, there exist two challenges in formulating and solving (3). Firstly, since the model is oblivious about the attack, it is impossible to determine how the adversarial input x' is generated, whether it has a corresponding clean input x , and what x is if it exists. As such, $u_i(t|x)$ is unknown, which serves as a clean reference in (3). We address this problem by inducing the notion of Neural Dynamic Signature (NDS), the neuron’s membrane potential averaged over a given clean training dataset \mathcal{D} , to provide an anchor for stabilizing membrane potential. Secondly, since externally generated attacks are not known *a priori*, it is desirable to suppress the perturbation of each neuron’s membrane potential in an online manner. For this, we propose a new type of spiking neurons, called threshold-adapting leaky integrate-and-fire (TA-LIF) neurons with a properly designed firing threshold voltage dynamics that serves as a homeostatic control to suppress undesirable membrane potential perturbations. We discuss these two techniques next.

3.2 Neural Dynamic Signature (NDS) as an Anchor

We utilize a clean training dataset \mathcal{D} to anchor each spiking neuron i . While the membrane potential $u_i(t|x)$ shows variability across individual samples x , its expected value over distribution \mathcal{D} denoted by $u_i^*(t|\mathcal{D})$ can act as a reliable reference as illustrated in Fig 1(a):

$$u_i^*(t|\mathcal{D}) \triangleq \mathbb{E}_{x \sim \mathcal{D}} [u_i(t|x)] \quad (4)$$

The Neural Dynamic Signature (NDS) of neuron i is defined as a temporal series vector over T timesteps: $\mathbf{u}_i^*(\mathcal{D}) = [u_i^*(t_1|\mathcal{D}), u_i^*(t_2|\mathcal{D}), \dots, u_i^*(t_T|\mathcal{D})]$. $\mathbf{u}_i^*(\mathcal{D})$ captures the average semantic

activation across \mathcal{D} . Adversarial perturbations induce input distributional shifts, leading to anomalous activation of out-of-distributional semantics. $\mathbf{u}_i^*(\mathcal{D})$ facilitates the identification of neuronal activation aberrations and further offers an anchor signal to bolster network resilience.

We also define the network-level NDS, $\mathcal{U}_{\text{NET}}(\mathcal{D}) \triangleq \{\mathbf{u}_i(\mathcal{D})\}_{i=1}^N$, as the collection of NDS vectors in a well-trained LIF-based SNN comprising N neurons. A densely populated SNN with N neurons typically has $O(N^2)$ weight parameters. In contrast, $\mathcal{U}_{\text{NET}}(\mathcal{D})$ scales as $O(NT)$. Recent algorithms have enabled training of high-accuracy SNNs with short latency operating over a small number of time steps, e.g., 5 to 10 [68]. Consequently, the storage overhead of NDS remains manageable.

Dynamics of NDS While serving as an anchor signal, the dynamics of NDS provides a basis for understanding the property of the proposed TA-LIF neurons. As NDS $u_i^*(t|\mathcal{D})$ of neuron i is derived from the well-trained LIF SNN, we take expectation of the LIF dynamic equation (1) with a static firing threshold V_{th} across the entire training distribution \mathcal{D} while simplifying the dynamics by approximating the effects of firing:

$$\tau_m \frac{du_i^*(t|\mathcal{D})}{dt} = -u_i^*(t|\mathcal{D}) + I_i^*(t|\mathcal{D}) - \tau_m r_i^*(\mathcal{D}) V_{th} \quad (5)$$

Here, $I_i^*(t|\mathcal{D})$ defines the average current input $\mathbb{E}_{x \sim \mathcal{D}}[I_i(t|\theta, x)]$, and $r_i^*(\mathcal{D})$ denotes the average firing rate $\mathbb{E}_{x \sim \mathcal{D}}[\int_0^{t_T} \frac{s_i(t|x)}{t_T} dt]$.

3.3 Threshold-Adapting Leaky Integrate-and-Fire (TA-LIF) Neurons

3.3.1 Membrane Potential Error Minimization with NDS

Instead of examining the deviation of membrane potential $u_i(t|x')$ caused by the adversarial input x' from the unknown $u_i(t|x)$, we define a new error signal $e_i(t|x') \triangleq u_i(t|x') - u_i^*(t|\mathcal{D})$, and replace the optimization problem of (3) by a more practical membrane potential error minimization problem while optimizing the dynamically changing firing threshold $V_{th}^i(t|x')$ of each neuron i :

$$\min_{\mathbf{V}_{th}^i \in \mathbb{R}^T} E_i(x') = \sum_{t=0}^T \frac{1}{2} e_i(t|x')^2 \triangleq \sum_{t=0}^T \frac{1}{2} (u_i(t|x') - u_i^*(t|\mathcal{D}))^2, \quad (6)$$

where $\mathbf{V}_{th}^i = [V_{th}^i(t_1|x'), V_{th}^i(t_2|x'), \dots, V_{th}^i(t_T|x')]$. The intrinsic parameter of firing threshold has a critical role in neuronal dynamics and spiking firing. Adapting the firing threshold can mitigate the effects of adversarial noise, and offer an online homeostatic mechanism for minimizing $E_i(x')$, which is potentially generalizable across various attack strengths and types.

3.3.2 Error Minimization of TA-LIF Neurons as a Second-Order Homeostatic Control System

Subtracting (5) from (1) gives the following dynamics of the error signal $e_i(t)$:

$$\tau_m \frac{de_i(t|x')}{dt} = -e_i(t|x') + \Delta I_i(t|x') - \tau_m [r_i(x') V_{th}^i(t|x') - r_i^*(\mathcal{D}) V_{th}], \quad (7)$$

where $\Delta I_i(t|x') \triangleq I_i(t|x') - I_i^*(t|\mathcal{D})$, and $r_i(x') \triangleq \int_0^{t_T} \frac{s_i(t|x')}{t_T} dt$ represents the average firing rate under the adversarial input x' . Differentiating (7) with respect to time and incorporating the threshold dynamics yields:

$$\tau_m \frac{d^2 e_i(t)}{dt^2} + \frac{de_i(t)}{dt} + r_i \tau_m \frac{dV_{th}^i(t)}{dt} = \varepsilon(t), \quad (8)$$

where $\varepsilon(t) \triangleq \frac{d\Delta I_i(t|x')}{dt}$, and we omit the notational dependencies on x' for clarity. Importantly, (8) characterizes the error dynamics $e_i(t)$ as a second-order control system influenced by the external disturbance $\varepsilon(t)$ with $\frac{dV_{th}^i(t)}{dt}$ serving as the control term.

We seek to solve the membrane potential error minimization problem in (6) by designing a control scheme that leads to proper error dynamics based on the second-order error system of (8). To this end, we utilize control signal $\frac{dV_{th}^i(t)}{dt}$ to provide a negative feedback control to suppress $e_i(t|x')$:

$$\frac{dV_{th}^i(t|x')}{dt} = \theta_i e_i(t|x') = \theta_i [u_i(t|x') - u_i^*(t|\mathcal{D})], \quad (9)$$

where θ_i is a neuron-level learnable parameter, dictating the pace of firing threshold adjustment.

TA-LIF model. (1), (2), and (9) together delineate the proposed TA-LIF model. We construct a homeostatic SNN (HoSNN) using TA-LIF neurons, where each TA-LIF neuron maintains its unique θ_i and $V_{th}^i(t)$. To extract precise semantic information from \mathcal{D} , we collect the NDS for the HoSNN from a well-trained LIF-SNN with identical network configurations. θ_i and network weights W of the HoSNN can be jointly optimized using a training algorithm such as backpropagation.

During inference with the optimized θ_i , $V_{th}^i(t)$ is adapted in an unsupervised manner according to (9). Intuitively, if TA-LIF neuron i shows abnormal increased activation relative to the reference NDS, $V_{th}^i(t)$ would be stepped up to suppress the increase in membrane potential. Conversely, if the neuron is abnormally inhibited, $V_{th}^i(t)$ would be tuned down. Figure 3 compares the LIF and TA-LIF models via numerical simulation of (8), showing the growth of error $e_i(t)$ over time. We set the $\varepsilon(t)$ as Gaussian white noise $\xi(t) \sim \mathcal{N}(0, 1)$ and repeated the simulation 1000 times. The membrane potential error of TA-LIF (red area) is significantly smaller than that of LIF (blue area), revealing TA-LIF’s dynamic robustness under noisy input perturbations.

The feedback control in (9) offers a straightforward means to implement homeostasis, which in turn enhances the adversarial resilience of the proposed HoSNNs. Furthermore, this homeostatic control exhibits two favorable dynamic properties presented next, underscoring its relevance in solving the membrane potential error minimization problem of (6) as a feedback control solution.

3.3.3 Theoretical Dynamic Properties of TA-LIF Neurons

We highlight key properties of the TA-LIF dynamics from two perspectives: bounded-input bounded-output (BIBO) stability of membrane potential error and suppressed time growth of error in comparison with the standard LIF model. See Appendix A B for a complete derivation of these properties.

BIBO Stability If a system is BIBO stable, then the output will be bounded for every input to the system that is bounded. The characteristic equation and its roots of the proposed second-order TA-LIF dynamics (8) incorporating the homeostatic control (9) are:

$$\tau_m s^2 + s + r_i \tau_m \theta_i = 0, \quad s_{1,2} = \frac{-1 \pm \sqrt{\Delta}}{2\tau_m}, \quad \Delta = 1 - 4r_i \tau_m^2 \theta_i \quad (10)$$

For a second-order system to be BIBO, the roots of its characteristic equation must be a negative real or have a negative real part, which is clearly the case for the TA-LIF model with $\theta_i > 0$ and $r_i > 0$, affirming the BIBO stability of the TA-LIF model. This signifies that when the adversarial input perturbation $\varepsilon(t)$ is bounded, the deviation of the TA-LIF neuron’s membrane potential $e_i(t)$ is also bounded, demonstrating the good control of error under various attack intensities.

Suppressed Time Growth of Membrane Potential Error To analyze evolution of membrane potential error induced by injected input perturbations over time, we follow the common practice [21, 1, 9, 49] to approximate $\Delta I(t)$ in (8) as a Wiener process, representing small, independent, and random perturbations. Consequently, the driving force $\varepsilon(t)$ on the right of (8) can be approximated by white noise $\xi(t)$ with zero mean and variance σ^2 . By the theory of stochastic differential equations [27], this leads to the following mean square error for the LIF and TA-LIF models, respectively:

$$\text{LIF} : \frac{dV_{th}^i}{dt} = 0 \implies \langle e_i^2(t) \rangle = \frac{\tau_m^2 \sigma^2}{2} (t - \tau_m + \tau_m e^{-t/\tau_m}) = O(\sigma^2 t) \quad (11)$$

$$\text{TA-LIF} : \frac{dV_{th}^i}{dt} = \theta_i e_i \implies \langle e_i^2(t) \rangle = \frac{\tau_m \sigma^2}{2r_i \theta_i} \left[1 - e^{-\frac{t}{\tau_m}} \left(\cos(\omega_1 t) + \frac{\sin(\omega_1 t)}{2\omega_1 \tau_m} \right) \right] = O(\sigma^2) \quad (12)$$

where $\omega_1 = \sqrt{r_i \theta_i - \frac{1}{4\tau_m^2}}$. Importantly, the mean square error of the TA-LIF neuron is $O(\sigma^2)$ and does not grow with time while that of LIF neurons grows unbounded with time. The suppression of time growth of membrane potential error by the TA-LIF model underscores its superiority over the LIF model in terms of adversarial robustness.

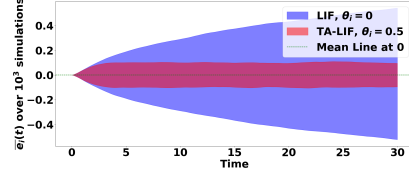


Figure 3: Numerical simulations of (8) show that TA-LIF can well suppress the growth of error with time. ($\tau_m = r = 1$)

3.4 Homeostatic SNNs (HoSNNs)

We introduce the homeostatic SNNs (HoSNNs), which deploy TA-LIF neurons as the basic compute units to leverage their noise immunity. Architecturally, HoSNNs can be constructed by adopting typical connectivity such as dense or convolutional layers, with two learnable parameters: synaptic weights \mathbf{W} and threshold dynamics parameter θ per (9). We extract the network-level NDS $\mathcal{U}_{\text{NET}}(\mathcal{D})$ from a LIF-based SNN with identical architecture well-trained on the clean data distribution \mathcal{D} . The HoSNNs optimization problem can be described as:

$$\mathbf{W}^*, \theta^* = \arg \min_{\mathbf{W}, \theta} \sum_{\{x, y\}} \mathcal{L}_{\text{train}}(x, y | \mathbf{W}, \theta, \mathbf{V}_{\text{th}}^*(x)) \quad (13)$$

$$\text{s.t. } \mathbf{V}_{\text{th}}^*(x) = \arg \min_{\mathbf{V}_{\text{th}}} \mathcal{L}_{\text{mem_error}}(\mathbf{W}, \theta, \mathbf{V}_{\text{th}}(x), \mathcal{U}_{\text{NET}}(\mathcal{D}) | x), \quad (14)$$

where x and y are an input/label pair; $\mathcal{L}_{\text{train}}(\cdot)$ is the loss over a training dataset that can include clean/adversarial examples, or a combination of the two; $\mathcal{L}_{\text{mem_error}} \triangleq \sum_{i=0}^N \sum_{t=0}^T \frac{1}{2} e_i(t|x)^2$ is the sum of all neurons' membrane potential error in (6). In practice, $\mathcal{L}_{\text{mem_error}}$ is optimized online by the homeostatic control of firing threshold during the forward process. $\mathcal{L}_{\text{train}}(\cdot)$ is optimized by gradient during the backward process, for which any backpropagation based training algorithm such as BPTT [43, 64], BPTR [31], or TSSL-BP [68] can be applied to optimize the network based on (13).

4 Experiments

4.1 Experimental Setup

The proposed HoSNNs are compared with LIF-based SNNs with identical architecture across four benchmark datasets: Fashion-MNIST (FMNIST) [65], Street View House Numbers (SVHN) [44] CIFAR10 and CIFAR100 [28]. VGG-like [55] convolutional neural network (CNN) architectures of different sizes and depths are utilized. Widely used methods including FGSM [22], RFGSM [58], PGD [36], and BIM [30] are used to generate both white-box and black-box attacks. The dynamically changing firing thresholds of the HoSNNs are exposed to the attacker and utilized in the gradient calculation when generating white-box attacks. We independently trained SNNs with the same architecture and used their white-box attacks as the black-box attacks to the HoSNNs.

For each HoSNN, an LIF-based SNN with an identical architecture is trained on the corresponding clean dataset to derive the NDS. Model training employs the BPTT learning algorithm ($T = 5$), leveraging a sigmoid surrogate gradient [67, 43, 64]. The learning rate for each θ_i in (9), which controls the adaptation of firing threshold of TA-LIF neurons, is set to 1/10 of that for the network weights, ensuring hyperparameter stability during training. We ensure that θ_i is non-negative during optimization. We train four types of models: SNNs and HoSNNs on a clean dataset and a weak FGSM-based adversarial training dataset, respectively. For FGSM adversarial training, we set the attack budget to $\epsilon = 2/255$ on FMNIST, SVHN and CIFAR10 as in [15] and $\epsilon = 4/255$ on CIFAR100 as in [29]. For iterative attacks (PGD & BIM), we adopt parameters $\alpha = \epsilon/3$ and $steps = 7$ in accordance with [15]. The experimental settings are detailed in the Appendix C.

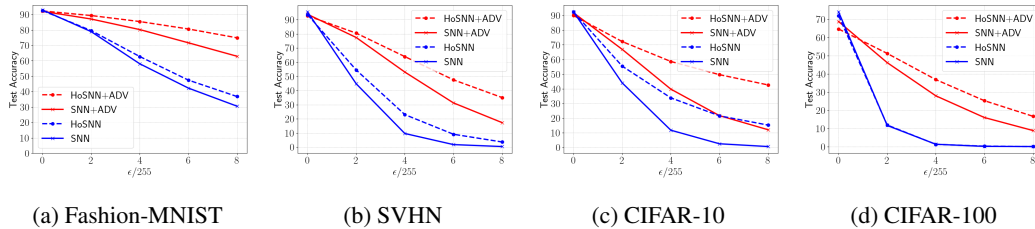


Figure 4: Performance of SNNs and HoSNNs as a function of white-box PGD attack intensity.

4.2 Adversarial Robustness under White-box Attacks

Accuracy under different PGD attack intensities Figure 4 shows model performance with and without adversarial training (ADV) under white-box PGD attacks with varying intensities:

$\epsilon = 2, 4, 6, 8/255$. The proposed HoSNNs consistently outperform the SNNs in terms of model accuracy across all attack intensities and four datasets. Additional results and ablation studies are provided in Table 1.

Robustness without adversarial training The left part of Table 1 compares HoSNNs and SNNs intrinsic resilience without adversarial training. Both types of network are trained exclusively on the clean dataset, and then subjected to $\epsilon = 8/255$ white-box adversarial attacks. The HoSNNs show consistently higher accuracy than the SNN counterparts under all four datasets and four attacks. For example, on CIFAR-10, the HoSNN significantly improves accuracy from 20.86% to 54.76% under FGSM attacks, and from 0.56% to 15.22% under PGD attacks.

Robustness with adversarial training In Table 1 right part, we evaluate the enhanced robustness of HoSNNs under adversarial training. We train both the SNNs and HoSNNs using FGSM adversarial training and then expose them to $\epsilon = 8/255$ white-box attacks. The results show a significant boost in robustness for HoSNNs when using adversarial training. Furthermore, the HoSNNs noticeably outperform the SNNs trained using the same FGSM adversarial training. For example, on CIFAR10, the HoSNNs improve the accuracy of the corresponding SNN to 63.98% from 37.93% under FGSM attack, and to 42.63% from 12.05% under PGD attack, respectively. On CIFAR100, the HoSNN improves the accuracy to 16.66% from 8.82% under PGD attack.

Table 1: Whitebox attack results on Fashion-MNIST, SVHN, CIFAR10 and CIFAR100 under various types of attack with an intensity of $\epsilon = 8/255$. The data on the left and right are based on training using the clean and weak FGSM datasets, respectively. The HoSNNs (denoted as \checkmark) provide greater robustness than the SNNs (denoted as \times) under all attacks and datasets.

Dataset	Net	Training on clean dataset					Training on $\epsilon = 2/255$ FGSM dataset				
		FGSM	RFGSM	PGD	BIM	Clean	FGSM	RFGSM	PGD	BIM	Clean
Fashion MNIST	\times	56.01	70.02	30.54	38.85	92.92	74.12	83.12	62.92	68.36	92.08
	\checkmark	65.36	76.10	35.79	49.02	92.96	84.7	87.99	74.91	79.61	92.31
SVHN	\times	26.07	42.94	0.44	2.26	95.51	48.37	68.81	17.36	30.09	93.85
	\checkmark	44.87	57.27	3.68	12.91	93.55	61.78	75.60	35.06	48.83	92.84
CIFAR 10	\times	20.86	38.72	0.56	3.29	92.47	37.93	59.50	12.05	22.31	91.87
	\checkmark	54.76	62.33	15.22	28.06	92.43	63.98	71.07	42.63	52.33	90.00
CIFAR 100	\times	5.74	8.94	0.04	0.10	74.00	22.54	36.93	8.82	13.58	68.72
	\checkmark	13.48	12.27	0.19	0.50	71.97	26.97	41.45	16.66	21.09	64.64

4.3 Adversarial Robustness under Black-box Attacks

Black Box Robustness Table 2 evaluates the robustness of SNNs (denoted as \times) and HoSNNs (denoted as \checkmark) against black-box attacks. All models are trained by weak FGSM adversarial training and tested by $\epsilon = 32/255$ black-box attacks generated using separately trained SNNs with identical architecture. Table 2 shows that the HoSNNs exhibit significantly stronger black-box robustness than the SNN counterparts. For example on CIFAR-10, the HoSNN outperforms the traditional SNN under the FGSM and PGD attacks with 11.7% and 13.31% accuracy improvements, respectively. On CIFAR-100, HoSNN improves the PGD accuracy from 6.74% to 16.90%.

Table 2: Blackbox attack results.

Dataset	Net	FGSM	RFGSM	PGD	BIM	Clean
Fashion MNIST	\times	66.26	80.09	74.08	73.43	92.08
	\checkmark	68.31	80.73	75.12	74.09	92.31
SVHN	\times	17.37	42.64	21.16	36.70	93.85
	\checkmark	19.08	44.57	25.97	40.75	92.84
CIFAR 10	\times	13.48	8.79	0.11	0.31	91.87
	\checkmark	25.18	31.11	13.42	23.34	90.00
CIFAR 100	\times	12.18	17.87	6.74	17.36	68.72
	\checkmark	14.54	24.32	16.90	32.04	64.64

Table 3: Comparison with others work

Data	Methods	FGSM	PGD	Clean
C-10	Sharmin et al.[53]	15.00	3.80	89.30
	Kundu et al.[29]	38.00	9.10	87.50
	Ding et al.[15]	45.23	21.16	90.74
	Our work	63.98	42.63	90.00
C-100	Sharmin et al.[53]	15.50	6.30	64.40
	Kundu et al.[29]	22.00	7.50	65.10
	Our work	26.97	16.66	64.64

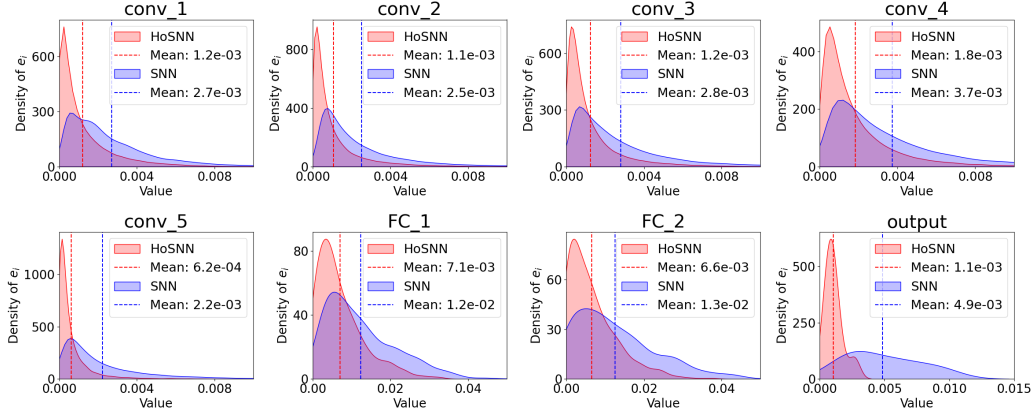


Figure 6: Distribution of post-synaptic current relative error of a SNN and HoSNN trained with FGSM adversarial training with $\epsilon = 2/255$ and attacked by black-box PGD attack with $\epsilon = 8/255$.

Layer-wise Relative Error of Post-synaptic Currents Perturbation in membrane potential caused by adversarial inputs can alter the output spike train of each neuron, and the resulting shifts in its post-synaptic current (PSC) can propagate through the successive layers. The PSC $a_i(t)$ is calculated by $\tau_s \frac{da_i(t)}{dt} = -a_i(t) + s_i(t)$ where τ_s is synaptic time constant. To reveal the source of HoSNNs robustness, we examine the relative error in PSC induced by adversarial attacks. On CIFAR10, we use the $\epsilon = 8/255$ black-box PGD attack to attack a SNN and HoSNN trained with the $\epsilon = 2/255$ FGSM adversarial training. For neuron i , we record its PSC $a_i(t)$ and $a'_i(t)$ under each pair of clean and adversarial input, respectively, and then calculate the difference of $e_i^{PSC}(t) \triangleq |a_i(t) - a'_i(t)|$ as an error metric. The layer-wise distributions of the relative error e_i^{PSC} are plotted in Figure 6. Each error distribution of the HoSNN has a significantly reduced mean compared with that of the SNN, and has its probability mass concentrated on low PSC error values, revealing the favorable internal self-stabilization introduced by the proposed homeostasis. Correspondingly, the HoSNN delivers an accuracy of 76.62%, significantly surpassing the 46.97% accuracy of the SNN.

4.4 Additional Experiments

Checklist for gradient obfuscation For a detailed check of **gradient obfuscation** [4, 10], we provide comprehensive inspection and data in Appendix D and E. The proposed HoSNNs pass all five tests including: (1) Single-step attacks do not perform better compared to iterative attacks (Fig 7). (2) Black-box attacks do not perform better compared to white-box attacks (Fig 8). (3) Increasing perturbation bound can increase attack strength. (4) Unbounded attacks can reach $\sim 100\%$ success (Fig 9) (5) Adversarial examples can't be found through random sampling as gradient attacks work.

Comparison with the works We compare our method against recent state-of-the-art defense methods under white-box FGSM and PGD attacks on CIFAR-10 and CIFAR-100 in Table 3. On CIFAR-10, our adversarially trained model achieved the highest defense accuracies of 63.98% and 42.63% for FGSM and PGD attacks, respectively. On CIFAR-100, our adversarially trained model achieved the highest defense accuracies of 26.97% and 16.66% under the two attacks, respectively.

5 Discussions

This paper presents the first work on biologically inspired homeostasis for enhancing adversarial robustness of spiking neural networks. Specifically, we propose a new TA-LIF model with a threshold adaptation mechanism and use TA-LIF neurons to construct inherently more robust HoSNN networks. Yet, there is room for future investigations including better trading off between model accuracy under clean and adversarial inputs. More broadly, we recognize the vast and yet untapped potential of biological homeostasis in neural network research. The relationship between the properties of individual neurons and the overall performance of the network warrants further exploration.

References

- [1] Larry F Abbott and Carl Van Vreeswijk. Asynchronous states in networks of pulse-coupled oscillators. *Physical Review E*, 48(2):1483, 1993.
- [2] Naveed Akhtar and Ajmal Mian. Threat of adversarial attacks on deep learning in computer vision: A survey. *Ieee Access*, 6:14410–14430, 2018.
- [3] AllenInstitute. *Allen Cell Types Database, cell feature search*. AllenInstitute, 2018.
- [4] Anish Athalye, Nicholas Carlini, and David Wagner. Obfuscated gradients give a false sense of security: Circumventing defenses to adversarial examples. In *International conference on machine learning*, pages 274–283. PMLR, 2018.
- [5] Guillaume Bellec, Darjan Salaj, Anand Subramoney, Robert Legenstein, and Wolfgang Maass. Long short-term memory and learning-to-learn in networks of spiking neurons. *Advances in neural information processing systems*, 31, 2018.
- [6] Guillaume Bellec, Franz Scherr, Anand Subramoney, Elias Hajek, Darjan Salaj, Robert Legenstein, and Wolfgang Maass. A solution to the learning dilemma for recurrent networks of spiking neurons. *Nature communications*, 11(1):3625, 2020.
- [7] Claude Bernard. *Introduction à l’étude de la médecine expérimentale*. Number 2. Baillière, 1865.
- [8] Battista Biggio and Fabio Roli. Wild patterns: Ten years after the rise of adversarial machine learning. In *Proceedings of the 2018 ACM SIGSAC Conference on Computer and Communications Security*, pages 2154–2156, 2018.
- [9] Nicolas Brunel. Dynamics of sparsely connected networks of excitatory and inhibitory spiking neurons. *Journal of computational neuroscience*, 8:183–208, 2000.
- [10] Nicholas Carlini, Anish Athalye, Nicolas Papernot, Wieland Brendel, Jonas Rauber, Dimitris Tsipras, Ian Goodfellow, Aleksander Madry, and Alexey Kurakin. On evaluating adversarial robustness, 2019.
- [11] Anirban Chakraborty, Manaar Alam, Vishal Dey, Anupam Chattopadhyay, and Debdeep Mukhopadhyay. Adversarial attacks and defences: A survey. *arXiv preprint arXiv:1810.00069*, 2018.
- [12] Sayeed Shafayet Chowdhury, Chankyu Lee, and Kaushik Roy. Towards understanding the effect of leak in spiking neural networks. *Neurocomputing*, 464:83–94, 2021.
- [13] Steven J Cooper. From claudes bernard to walter cannon. emergence of the concept of homeostasis. *Appetite*, 51(3):419–427, 2008.
- [14] Lei Deng, Yujie Wu, Xing Hu, Ling Liang, Yufei Ding, Guoqi Li, Guangshe Zhao, Peng Li, and Yuan Xie. Rethinking the performance comparison between snns and anns. *Neural networks*, 121:294–307, 2020.
- [15] Jianhao Ding, Tong Bu, Zhaofei Yu, Tiejun Huang, and Jian Liu. Snn-rat: Robustness-enhanced spiking neural network through regularized adversarial training. *Advances in Neural Information Processing Systems*, 35:24780–24793, 2022.
- [16] Rida El-Allami, Alberto Marchisio, Muhammad Shafique, and Ihsen Alouani. Securing deep spiking neural networks against adversarial attacks through inherent structural parameters. In *2021 Design, Automation & Test in Europe Conference & Exhibition (DATE)*, pages 774–779. IEEE, 2021.
- [17] Alhussein Fawzi, Seyed-Mohsen Moosavi-Dezfooli, and Pascal Frossard. Robustness of classifiers: from adversarial to random noise. *Advances in neural information processing systems*, 29, 2016.
- [18] Nic Ford, Justin Gilmer, Nicholas Carlini, and Dogus Cubuk. Adversarial examples are a natural consequence of test error in noise. *arXiv preprint arXiv:1901.10513*, 2019.

- [19] Steve B Furber, Francesco Galluppi, Steve Temple, and Luis A Plana. The spinnaker project. *Proceedings of the IEEE*, 102(5):652–665, 2014.
- [20] Wulfram Gerstner and Werner M Kistler. *Spiking neuron models: Single neurons, populations, plasticity*. Cambridge university press, 2002.
- [21] Wulfram Gerstner, Werner M Kistler, Richard Naud, and Liam Paninski. *Neuronal dynamics: From single neurons to networks and models of cognition*. Cambridge University Press, 2014.
- [22] Ian J Goodfellow, Jonathon Shlens, and Christian Szegedy. Explaining and harnessing adversarial examples. *arXiv preprint arXiv:1412.6572*, 2014.
- [23] Andrew Ilyas, Shibani Santurkar, Dimitris Tsipras, Logan Engstrom, Brandon Tran, and Aleksander Madry. Adversarial examples are not bugs, they are features. *Advances in neural information processing systems*, 32, 2019.
- [24] Nabil Imam and Thomas A Cleland. Rapid online learning and robust recall in a neuromorphic olfactory circuit. *Nature Machine Intelligence*, 2(3):181–191, 2020.
- [25] Wilfrid Jänig. *The integrative action of the autonomic nervous system: neurobiology of homeostasis*. Cambridge University Press, 2022.
- [26] Daniel Kang, Yi Sun, Dan Hendrycks, Tom Brown, and Jacob Steinhardt. Testing robustness against unforeseen adversaries. *arXiv preprint arXiv:1908.08016*, 2019.
- [27] Peter E Kloeden, Eckhard Platen, Peter E Kloeden, and Eckhard Platen. *Stochastic differential equations*. Springer, 1992.
- [28] Alex Krizhevsky. Learning multiple layers of features from tiny images. Technical report, Citeseer, 2009.
- [29] Souvik Kundu, Massoud Pedram, and Peter A Beerel. Hire-snn: Harnessing the inherent robustness of energy-efficient deep spiking neural networks by training with crafted input noise. In *Proceedings of the IEEE/CVF International Conference on Computer Vision*, pages 5209–5218, 2021.
- [30] Alexey Kurakin, Ian J Goodfellow, and Samy Bengio. Adversarial examples in the physical world. In *Artificial intelligence safety and security*, pages 99–112. Chapman and Hall/CRC, 2018.
- [31] Chankyu Lee, Syed Shakib Sarwar, Priyadarshini Panda, Gopalakrishnan Srinivasan, and Kaushik Roy. Enabling spike-based backpropagation for training deep neural network architectures. *Frontiers in neuroscience*, page 119, 2020.
- [32] Tianlin Li, Aishan Liu, Xianglong Liu, Yitao Xu, Chongzhi Zhang, and Xiaofei Xie. Understanding adversarial robustness via critical attacking route. *Information Sciences*, 547:568–578, 2021.
- [33] Yanjie Li, Xiaoxin Cui, Yihao Zhou, and Ying Li. A comparative study on the performance and security evaluation of spiking neural networks. *IEEE Access*, 10:117572–117581, 2022.
- [34] Ling Liang, Kaidi Xu, Xing Hu, Lei Deng, and Yuan Xie. Toward robust spiking neural network against adversarial perturbation. *Advances in Neural Information Processing Systems*, 35: 10244–10256, 2022.
- [35] Timothy P Lillicrap, Adam Santoro, Luke Marris, Colin J Akerman, and Geoffrey Hinton. Backpropagation and the brain. *Nature Reviews Neuroscience*, 21(6):335–346, 2020.
- [36] Aleksander Madry, Aleksandar Makelov, Ludwig Schmidt, Dimitris Tsipras, and Adrian Vladu. Towards deep learning models resistant to adversarial attacks. *arXiv preprint arXiv:1706.06083*, 2017.
- [37] Eve Marder and Jean-Marc Goillaud. Variability, compensation and homeostasis in neuron and network function. *Nature Reviews Neuroscience*, 7(7):563–574, 2006.

- [38] Jan Hendrik Metzen, Tim Genewein, Volker Fischer, and Bastian Bischoff. On detecting adversarial perturbations. *arXiv preprint arXiv:1702.04267*, 2017.
- [39] Harold Modell, William Cliff, Joel Michael, Jenny McFarland, Mary Pat Wenderoth, and Ann Wright. A physiologist’s view of homeostasis. *Advances in physiology education*, 2015.
- [40] Seyed-Mohsen Moosavi-Dezfooli, Alhussein Fawzi, and Pascal Frossard. Deepfool: a simple and accurate method to fool deep neural networks. In *Proceedings of the IEEE conference on computer vision and pattern recognition*, pages 2574–2582, 2016.
- [41] Aamir Mustafa, Salman Khan, Munawar Hayat, Roland Goecke, Jianbing Shen, and Ling Shao. Adversarial defense by restricting the hidden space of deep neural networks. In *Proceedings of the IEEE/CVF International Conference on Computer Vision*, pages 3385–3394, 2019.
- [42] Kaveri Nadhamuni. *Adversarial Examples and Distribution Shift: A Representations Perspective*. PhD thesis, Massachusetts Institute of Technology, 2021.
- [43] Emre O Neftci, Hesham Mostafa, and Friedemann Zenke. Surrogate gradient learning in spiking neural networks: Bringing the power of gradient-based optimization to spiking neural networks. *IEEE Signal Processing Magazine*, 36(6):51–63, 2019.
- [44] Yuval Netzer, Tao Wang, Adam Coates, Alessandro Bissacco, Bo Wu, and Andrew Y Ng. Reading digits in natural images with unsupervised feature learning. 2011.
- [45] Katsuhiko Ogata. *Modern control engineering fifth edition*. 2010.
- [46] Jing Pei, Lei Deng, Sen Song, Mingguo Zhao, Youhui Zhang, Shuang Wu, Guanrui Wang, Zhe Zou, Zhenzhi Wu, Wei He, et al. Towards artificial general intelligence with hybrid tianjic chip architecture. *Nature*, 572(7767):106–111, 2019.
- [47] Sergio Pennazio. Homeostasis: a history of biology. In *Biology Forum/Rivista di Biologia*, volume 102, 2009.
- [48] Stephan Rabanser, Stephan Günnemann, and Zachary Lipton. Failing loudly: An empirical study of methods for detecting dataset shift. *Advances in Neural Information Processing Systems*, 32, 2019.
- [49] Alfonso Renart, Nicolas Brunel, and Xiao-Jing Wang. Mean-field theory of irregularly spiking neuronal populations and working memory in recurrent cortical networks. *Computational neuroscience: A comprehensive approach*, pages 431–490, 2004.
- [50] H. Risken. *The Fokker-Planck Equation: Methods of Solution and Applications*. Springer, New York, 2 edition, 1996. doi: 10.1007/978-3-642-61544-3_4.
- [51] Ramprasaath R. Selvaraju, Michael Cogswell, Abhishek Das, Ramakrishna Vedantam, Devi Parikh, and Dhruv Batra. Grad-cam: Visual explanations from deep networks via gradient-based localization. *International Journal of Computer Vision*, 128(2):336–359, October 2019. ISSN 1573-1405. doi: 10.1007/s11263-019-01228-7. URL <http://dx.doi.org/10.1007/s11263-019-01228-7>.
- [52] Saima Sharmin, Priyadarshini Panda, Syed Shakib Sarwar, Chankyu Lee, Wachirawit Ponghiran, and Kaushik Roy. A comprehensive analysis on adversarial robustness of spiking neural networks. In *2019 International Joint Conference on Neural Networks (IJCNN)*, pages 1–8. IEEE, 2019.
- [53] Saima Sharmin, Nitin Rathi, Priyadarshini Panda, and Kaushik Roy. Inherent adversarial robustness of deep spiking neural networks: Effects of discrete input encoding and non-linear activations. In *Computer Vision–ECCV 2020: 16th European Conference, Glasgow, UK, August 23–28, 2020, Proceedings, Part XXIX 16*, pages 399–414. Springer, 2020.
- [54] Manli Shu, Zuxuan Wu, Micah Goldblum, and Tom Goldstein. Prepare for the worst: Generalizing across domain shifts with adversarial batch normalization. 2020.

- [55] Karen Simonyan and Andrew Zisserman. Very deep convolutional networks for large-scale image recognition. In *Proceedings of the international conference on learning representations (ICLR)*, 2015.
- [56] Christian Szegedy, Wojciech Zaremba, Ilya Sutskever, Joan Bruna, Dumitru Erhan, Ian Goodfellow, and Rob Fergus. Intriguing properties of neural networks. *arXiv preprint arXiv:1312.6199*, 2013.
- [57] Corinne Teeter, Ramakrishnan Iyer, Vilas Menon, Nathan Gouwens, David Feng, Jim Berg, Aaron Szafer, Nicholas Cain, Hongkui Zeng, Michael Hawrylycz, et al. Generalized leaky integrate-and-fire models classify multiple neuron types. *Nature communications*, 9(1):709, 2018.
- [58] Florian Tramèr, Alexey Kurakin, Nicolas Papernot, Ian Goodfellow, Dan Boneh, and Patrick McDaniel. Ensemble adversarial training: Attacks and defenses. *arXiv preprint arXiv:1705.07204*, 2017.
- [59] Gina G Turrigiano and Sacha B Nelson. Homeostatic plasticity in the developing nervous system. *Nature reviews neuroscience*, 5(2):97–107, 2004.
- [60] George E Uhlenbeck and Leonard S Ornstein. On the theory of the brownian motion. *Physical review*, 36(5):823, 1930.
- [61] Nicolaas Godfried Van Kampen. *Stochastic processes in physics and chemistry*, volume 1. Elsevier, 1992.
- [62] Ming Chen Wang and George Eugene Uhlenbeck. On the theory of the brownian motion ii. *Reviews of modern physics*, 17(2-3):323, 1945.
- [63] H Arthur Woods and J Keaton Wilson. An information hypothesis for the evolution of homeostasis. *Trends in ecology & evolution*, 28(5):283–289, 2013.
- [64] Yujie Wu, Lei Deng, Guoqi Li, Jun Zhu, and Luping Shi. Spatio-temporal backpropagation for training high-performance spiking neural networks. *Frontiers in neuroscience*, 12:331, 2018.
- [65] Han Xiao, Kashif Rasul, and Roland Vollgraf. Fashion-mnist: a novel image dataset for benchmarking machine learning algorithms. *arXiv preprint arXiv:1708.07747*, 2017.
- [66] Cihang Xie, Jianyu Wang, Zhishuai Zhang, Zhou Ren, and Alan Yuille. Mitigating adversarial effects through randomization. *arXiv preprint arXiv:1711.01991*, 2017.
- [67] Nuo Xu, Kaleel Mahmood, Haowen Fang, Ethan Rathbun, Caiwen Ding, and Wujie Wen. Securing the spike: On the transferability and security of spiking neural networks to adversarial examples. *arXiv preprint arXiv:2209.03358*, 2022.
- [68] Wenrui Zhang and Peng Li. Temporal spike sequence learning via backpropagation for deep spiking neural networks. *Advances in Neural Information Processing Systems*, 33:12022–12033, 2020.

NeurIPS Paper Checklist

1. Claims

Question: Do the main claims made in the abstract and introduction accurately reflect the paper’s contributions and scope?

Answer: [\[Yes\]](#)

Justification: We clearly describe the motivation, main methods, and results of the study in the abstract and introduction.

Guidelines:

- The answer NA means that the abstract and introduction do not include the claims made in the paper.

- The abstract and/or introduction should clearly state the claims made, including the contributions made in the paper and important assumptions and limitations. A No or NA answer to this question will not be perceived well by the reviewers.
- The claims made should match theoretical and experimental results, and reflect how much the results can be expected to generalize to other settings.
- It is fine to include aspirational goals as motivation as long as it is clear that these goals are not attained by the paper.

2. Limitations

Question: Does the paper discuss the limitations of the work performed by the authors?

Answer: [Yes]

Justification: We discuss the limitations in the Discussion section.

Guidelines:

- The answer NA means that the paper has no limitation while the answer No means that the paper has limitations, but those are not discussed in the paper.
- The authors are encouraged to create a separate "Limitations" section in their paper.
- The paper should point out any strong assumptions and how robust the results are to violations of these assumptions (e.g., independence assumptions, noiseless settings, model well-specification, asymptotic approximations only holding locally). The authors should reflect on how these assumptions might be violated in practice and what the implications would be.
- The authors should reflect on the scope of the claims made, e.g., if the approach was only tested on a few datasets or with a few runs. In general, empirical results often depend on implicit assumptions, which should be articulated.
- The authors should reflect on the factors that influence the performance of the approach. For example, a facial recognition algorithm may perform poorly when image resolution is low or images are taken in low lighting. Or a speech-to-text system might not be used reliably to provide closed captions for online lectures because it fails to handle technical jargon.
- The authors should discuss the computational efficiency of the proposed algorithms and how they scale with dataset size.
- If applicable, the authors should discuss possible limitations of their approach to address problems of privacy and fairness.
- While the authors might fear that complete honesty about limitations might be used by reviewers as grounds for rejection, a worse outcome might be that reviewers discover limitations that aren't acknowledged in the paper. The authors should use their best judgment and recognize that individual actions in favor of transparency play an important role in developing norms that preserve the integrity of the community. Reviewers will be specifically instructed to not penalize honesty concerning limitations.

3. Theory Assumptions and Proofs

Question: For each theoretical result, does the paper provide the full set of assumptions and a complete (and correct) proof?

Answer: [Yes]

Justification: We provide all assumptions and the complete proof in Appendix A.

Guidelines:

- The answer NA means that the paper does not include theoretical results.
- All the theorems, formulas, and proofs in the paper should be numbered and cross-referenced.
- All assumptions should be clearly stated or referenced in the statement of any theorems.
- The proofs can either appear in the main paper or the supplemental material, but if they appear in the supplemental material, the authors are encouraged to provide a short proof sketch to provide intuition.
- Inversely, any informal proof provided in the core of the paper should be complemented by formal proofs provided in appendix or supplemental material.

- Theorems and Lemmas that the proof relies upon should be properly referenced.

4. Experimental Result Reproducibility

Question: Does the paper fully disclose all the information needed to reproduce the main experimental results of the paper to the extent that it affects the main claims and/or conclusions of the paper (regardless of whether the code and data are provided or not)?

Answer: [Yes]

Justification: See experimental setting in main paper and Appendix C.

Guidelines:

- The answer NA means that the paper does not include experiments.
- If the paper includes experiments, a No answer to this question will not be perceived well by the reviewers: Making the paper reproducible is important, regardless of whether the code and data are provided or not.
- If the contribution is a dataset and/or model, the authors should describe the steps taken to make their results reproducible or verifiable.
- Depending on the contribution, reproducibility can be accomplished in various ways. For example, if the contribution is a novel architecture, describing the architecture fully might suffice, or if the contribution is a specific model and empirical evaluation, it may be necessary to either make it possible for others to replicate the model with the same dataset, or provide access to the model. In general, releasing code and data is often one good way to accomplish this, but reproducibility can also be provided via detailed instructions for how to replicate the results, access to a hosted model (e.g., in the case of a large language model), releasing of a model checkpoint, or other means that are appropriate to the research performed.
- While NeurIPS does not require releasing code, the conference does require all submissions to provide some reasonable avenue for reproducibility, which may depend on the nature of the contribution. For example
 - (a) If the contribution is primarily a new algorithm, the paper should make it clear how to reproduce that algorithm.
 - (b) If the contribution is primarily a new model architecture, the paper should describe the architecture clearly and fully.
 - (c) If the contribution is a new model (e.g., a large language model), then there should either be a way to access this model for reproducing the results or a way to reproduce the model (e.g., with an open-source dataset or instructions for how to construct the dataset).
 - (d) We recognize that reproducibility may be tricky in some cases, in which case authors are welcome to describe the particular way they provide for reproducibility. In the case of closed-source models, it may be that access to the model is limited in some way (e.g., to registered users), but it should be possible for other researchers to have some path to reproducing or verifying the results.

5. Open access to data and code

Question: Does the paper provide open access to the data and code, with sufficient instructions to faithfully reproduce the main experimental results, as described in supplemental material?

Answer: [Yes]

Justification: We provide the code and model weights.

Guidelines:

- The answer NA means that paper does not include experiments requiring code.
- Please see the NeurIPS code and data submission guidelines (<https://nips.cc/public/guides/CodeSubmissionPolicy>) for more details.
- While we encourage the release of code and data, we understand that this might not be possible, so “No” is an acceptable answer. Papers cannot be rejected simply for not including code, unless this is central to the contribution (e.g., for a new open-source benchmark).

- The instructions should contain the exact command and environment needed to run to reproduce the results. See the NeurIPS code and data submission guidelines (<https://nips.cc/public/guides/CodeSubmissionPolicy>) for more details.
- The authors should provide instructions on data access and preparation, including how to access the raw data, preprocessed data, intermediate data, and generated data, etc.
- The authors should provide scripts to reproduce all experimental results for the new proposed method and baselines. If only a subset of experiments are reproducible, they should state which ones are omitted from the script and why.
- At submission time, to preserve anonymity, the authors should release anonymized versions (if applicable).
- Providing as much information as possible in supplemental material (appended to the paper) is recommended, but including URLs to data and code is permitted.

6. Experimental Setting/Details

Question: Does the paper specify all the training and test details (e.g., data splits, hyper-parameters, how they were chosen, type of optimizer, etc.) necessary to understand the results?

Answer: [Yes]

Justification: See experimental setting in main paper and Appendix C.

Guidelines:

- The answer NA means that the paper does not include experiments.
- The experimental setting should be presented in the core of the paper to a level of detail that is necessary to appreciate the results and make sense of them.
- The full details can be provided either with the code, in appendix, or as supplemental material.

7. Experiment Statistical Significance

Question: Does the paper report error bars suitably and correctly defined or other appropriate information about the statistical significance of the experiments?

Answer: [No]

Justification: Code and model weights have been provided to reproduce the experiment.

Guidelines:

- The answer NA means that the paper does not include experiments.
- The authors should answer "Yes" if the results are accompanied by error bars, confidence intervals, or statistical significance tests, at least for the experiments that support the main claims of the paper.
- The factors of variability that the error bars are capturing should be clearly stated (for example, train/test split, initialization, random drawing of some parameter, or overall run with given experimental conditions).
- The method for calculating the error bars should be explained (closed form formula, call to a library function, bootstrap, etc.)
- The assumptions made should be given (e.g., Normally distributed errors).
- It should be clear whether the error bar is the standard deviation or the standard error of the mean.
- It is OK to report 1-sigma error bars, but one should state it. The authors should preferably report a 2-sigma error bar than state that they have a 96% CI, if the hypothesis of Normality of errors is not verified.
- For asymmetric distributions, the authors should be careful not to show in tables or figures symmetric error bars that would yield results that are out of range (e.g. negative error rates).
- If error bars are reported in tables or plots, The authors should explain in the text how they were calculated and reference the corresponding figures or tables in the text.

8. Experiments Compute Resources

Question: For each experiment, does the paper provide sufficient information on the computer resources (type of compute workers, memory, time of execution) needed to reproduce the experiments?

Answer: [Yes]

Justification: See Appendix C.

Guidelines:

- The answer NA means that the paper does not include experiments.
- The paper should indicate the type of compute workers CPU or GPU, internal cluster, or cloud provider, including relevant memory and storage.
- The paper should provide the amount of compute required for each of the individual experimental runs as well as estimate the total compute.
- The paper should disclose whether the full research project required more compute than the experiments reported in the paper (e.g., preliminary or failed experiments that didn't make it into the paper).

9. Code Of Ethics

Question: Does the research conducted in the paper conform, in every respect, with the NeurIPS Code of Ethics <https://neurips.cc/public/EthicsGuidelines?>

Answer: [Yes]

Justification: Yes, we conform with the NeurIPS Code of Ethics.

Guidelines:

- The answer NA means that the authors have not reviewed the NeurIPS Code of Ethics.
- If the authors answer No, they should explain the special circumstances that require a deviation from the Code of Ethics.
- The authors should make sure to preserve anonymity (e.g., if there is a special consideration due to laws or regulations in their jurisdiction).

10. Broader Impacts

Question: Does the paper discuss both potential positive societal impacts and negative societal impacts of the work performed?

Answer: [Yes]

Justification: See Introduction and Discussion .

Guidelines:

- The answer NA means that there is no societal impact of the work performed.
- If the authors answer NA or No, they should explain why their work has no societal impact or why the paper does not address societal impact.
- Examples of negative societal impacts include potential malicious or unintended uses (e.g., disinformation, generating fake profiles, surveillance), fairness considerations (e.g., deployment of technologies that could make decisions that unfairly impact specific groups), privacy considerations, and security considerations.
- The conference expects that many papers will be foundational research and not tied to particular applications, let alone deployments. However, if there is a direct path to any negative applications, the authors should point it out. For example, it is legitimate to point out that an improvement in the quality of generative models could be used to generate deepfakes for disinformation. On the other hand, it is not needed to point out that a generic algorithm for optimizing neural networks could enable people to train models that generate Deepfakes faster.
- The authors should consider possible harms that could arise when the technology is being used as intended and functioning correctly, harms that could arise when the technology is being used as intended but gives incorrect results, and harms following from (intentional or unintentional) misuse of the technology.
- If there are negative societal impacts, the authors could also discuss possible mitigation strategies (e.g., gated release of models, providing defenses in addition to attacks, mechanisms for monitoring misuse, mechanisms to monitor how a system learns from feedback over time, improving the efficiency and accessibility of ML).

11. Safeguards

Question: Does the paper describe safeguards that have been put in place for responsible release of data or models that have a high risk for misuse (e.g., pretrained language models, image generators, or scraped datasets)?

Answer: [NA]

Justification: The paper poses no such risks.

Guidelines:

- The answer NA means that the paper poses no such risks.
- Released models that have a high risk for misuse or dual-use should be released with necessary safeguards to allow for controlled use of the model, for example by requiring that users adhere to usage guidelines or restrictions to access the model or implementing safety filters.
- Datasets that have been scraped from the Internet could pose safety risks. The authors should describe how they avoided releasing unsafe images.
- We recognize that providing effective safeguards is challenging, and many papers do not require this, but we encourage authors to take this into account and make a best faith effort.

12. Licenses for existing assets

Question: Are the creators or original owners of assets (e.g., code, data, models), used in the paper, properly credited and are the license and terms of use explicitly mentioned and properly respected?

Answer: [Yes]

Justification: Yes we do. Our code is adapted from here

Guidelines:

- The answer NA means that the paper does not use existing assets.
- The authors should cite the original paper that produced the code package or dataset.
- The authors should state which version of the asset is used and, if possible, include a URL.
- The name of the license (e.g., CC-BY 4.0) should be included for each asset.
- For scraped data from a particular source (e.g., website), the copyright and terms of service of that source should be provided.
- If assets are released, the license, copyright information, and terms of use in the package should be provided. For popular datasets, paperswithcode.com/datasets has curated licenses for some datasets. Their licensing guide can help determine the license of a dataset.
- For existing datasets that are re-packaged, both the original license and the license of the derived asset (if it has changed) should be provided.
- If this information is not available online, the authors are encouraged to reach out to the asset's creators.

13. New Assets

Question: Are new assets introduced in the paper well documented and is the documentation provided alongside the assets?

Answer: [Yes]

Justification: Yes, we provide the code and model weights.

Guidelines:

- The answer NA means that the paper does not release new assets.
- Researchers should communicate the details of the dataset/code/model as part of their submissions via structured templates. This includes details about training, license, limitations, etc.
- The paper should discuss whether and how consent was obtained from people whose asset is used.

- At submission time, remember to anonymize your assets (if applicable). You can either create an anonymized URL or include an anonymized zip file.

14. Crowdsourcing and Research with Human Subjects

Question: For crowdsourcing experiments and research with human subjects, does the paper include the full text of instructions given to participants and screenshots, if applicable, as well as details about compensation (if any)?

Answer: [NA]

Justification: The paper does not involve crowdsourcing nor research with human subjects.

Guidelines:

- The answer NA means that the paper does not involve crowdsourcing nor research with human subjects.
- Including this information in the supplemental material is fine, but if the main contribution of the paper involves human subjects, then as much detail as possible should be included in the main paper.
- According to the NeurIPS Code of Ethics, workers involved in data collection, curation, or other labor should be paid at least the minimum wage in the country of the data collector.

15. Institutional Review Board (IRB) Approvals or Equivalent for Research with Human Subjects

Question: Does the paper describe potential risks incurred by study participants, whether such risks were disclosed to the subjects, and whether Institutional Review Board (IRB) approvals (or an equivalent approval/review based on the requirements of your country or institution) were obtained?

Answer: [NA]

Justification: The paper does not involve crowdsourcing nor research with human subjects.

Guidelines:

- The answer NA means that the paper does not involve crowdsourcing nor research with human subjects.
- Depending on the country in which research is conducted, IRB approval (or equivalent) may be required for any human subjects research. If you obtained IRB approval, you should clearly state this in the paper.
- We recognize that the procedures for this may vary significantly between institutions and locations, and we expect authors to adhere to the NeurIPS Code of Ethics and the guidelines for their institution.
- For initial submissions, do not include any information that would break anonymity (if applicable), such as the institution conducting the review.

Appendix / supplemental material

We mainly present the derivation of the second-order dynamic equation of TA-LIF in A, dynamic stability analysis in B the detailed experimental setup in C and checklist for gradient obfuscation in D the more data in E.

A Derivation of TA-LIF Dynamic Equation

In this section, we derive the approximate second-order dynamic equations of the threshold-adapting leaky integrate-and-fire (TA-LIF) neurons and subsequently analyze them.

A.1 LIF Dynamics

To facilitate our discussion, let's commence by presenting the first-order dynamic equations of the LIF neuron i at time t :

$$\tau_m \frac{du_i(t)}{dt} = -u_i(t) + I_i(t) - \tau_m s_i(t) V_{th} \quad (15)$$

The input current is defined as

$$I_i(t) = R \sum_j w_{ij} a_j(t) \quad (16)$$

The spiking behavior $s_i(t)$ is defined as:

$$s_i(t) = \begin{cases} +\infty & \text{if } u_i(t) \geq V_{th} \\ 0 & \text{otherwise} \end{cases} = \sum_f \delta(t - t_i^f) \quad (17)$$

And the post-synaptic current dynamics are given by:

$$\tau_s \frac{da_j(t)}{dt} = -a_j(t) + s_j(t) \quad (18)$$

Where:

- τ_m : Represents the membrane time constant.
- $I_i(t)$: Denotes the input, which is the summation of the pre-synaptic currents.
- w_{ij} : Stands for the synaptic weight from neuron j to neuron i .
- $a_j(t)$: Refers to the post-synaptic current induced by neuron j at time t .
- V_{th} : Is the static firing threshold.
- t_i^f : Indicates the f -th spike time of neuron i .
- τ_s : Is the synaptic time constant.

A.2 Neural Dynamic Signature

Let's begin by reviewing the definition of the Neural Dynamic Signature (NDS). Given a data instance x sampled from distribution \mathcal{D} , the NDS of neuron i , contingent upon the training set distribution \mathcal{D} , can be represented as a temporal series vector $\mathbf{u}_i^*(\mathcal{D})$. Specifically, at time t , it holds the value:

$$u_i^*(t|\mathcal{D}) \triangleq \mathbb{E}_{x \sim \mathcal{D}}[u_i(t|x)], \text{ for } t \in [0, T] \quad (19)$$

To derive the dynamics of NDS, we start by revisiting Equation (15), rewriting it with respect to x

$$\tau_m \frac{du_i(t|x)}{dt} = -u_i(t|x) + I_i(t|x) - \tau_m s_i(t|x) V_{th} \quad (20)$$

For the convenience of dynamic analysis, we choose to approximate the discontinuous Dirac function term $s_i(t|x)$ with the average firing rate $r_i(x)$ of neuron i . The average firing rate is calculated by

$$r_i(x) \triangleq \int_0^T \frac{s_i(t|x)}{T} dt \quad (21)$$

We take this approximation to address discontinuity of Dirac function, as $r_i(x)$ and $s_i(t|x)$ have the same integral value over time: the number of neuron firings. Substituting Equation (21) into Equation (20) and computing the expectation on both sides, we have:

$$\tau_m \mathbb{E}_{x \sim \mathcal{D}} \left[\frac{du_i(t|x)}{dt} \right] = -\mathbb{E}_{x \sim \mathcal{D}} [u_i(t|x)] + \mathbb{E}_{x \sim \mathcal{D}} [I_i(t|x)] - \tau_m \mathbb{E}_{x \sim \mathcal{D}} [r_i(x)] V_{th} \quad (22)$$

Here, we denote the average input current of neuron i over the entire dataset as:

$$I_i^*(t|\mathcal{D}) \triangleq \mathbb{E}_{x \sim \mathcal{D}} [I_i(t|x)] \quad (23)$$

and the average spike frequency of neuron i over the entire dataset as:

$$r_i^*(\mathcal{D}) \triangleq \mathbb{E}_{x \sim \mathcal{D}} [r_i(x)] \quad (24)$$

With the definition from Equation (19), the dynamics of NDS can be expressed as:

$$\tau_m \frac{du_i^*(t|\mathcal{D})}{dt} = -u_i^*(t|\mathcal{D}) + I_i^*(t|\mathcal{D}) - \tau_m r_i^*(\mathcal{D}) V_{th} \quad (25)$$

As mentioned in the main text, we usually expect NDS to have precise semantic information of the distribution \mathcal{D} . So NDS should be obtained through a well-trained model with optimal weight parameter \mathbf{W}^* . For clarity in the following sections, we use \mathbf{W}^* to represent the actually used NDS:

$$\tau_m \frac{du_i^*(t|\mathbf{W}^*, \mathcal{D})}{dt} = -u_i^*(t|\mathbf{W}^*, \mathcal{D}) + I_i^*(t|\mathbf{W}^*, \mathcal{D}) - \tau_m r_i^*(\mathbf{W}^*, \mathcal{D}) V_{th} \quad (26)$$

A.3 TA-LIF Dynamics

In this section, we delve deeper into the dynamical equations governing the TA-LIF neuron and derive its second-order dynamic equation

$$\tau_m \frac{du_i(t)}{dt} = -u_i(t) + I_i(t) - \tau_m s_i(t) V_{th}^i(t) \quad (27)$$

The synaptic input $I_i(t)$, the spike generation function $s_i(t)$ and post-synaptic current dynamics of TA-LIF are defined same as (16)(17)(18). For a specific network parameter \mathbf{W} and a sample x' drawn from \mathcal{D}' , the dynamic equation governing the threshold $V_{th}^i(t)$ is:

$$\frac{dV_{th}^i(t|\mathbf{W}, x')}{dt} = \theta_i e_i(t|\mathbf{W}, x'), \quad (28)$$

where the error signal, utilizing the NDS as given in (19), is defined as:

$$e_i(t|\mathbf{W}, x') \triangleq u_i(t|\mathbf{W}, x') - u_i^*(t|\mathbf{W}^*, \mathcal{D}) \quad (29)$$

Applying the continuity approximation for the Dirac function as per (21) and incorporating the conditional dependency of \mathbf{W} and x' , rewriting the dynamics for TA-LIF (27) as:

$$\tau_m \frac{du_i(t|\mathbf{W}, x')}{dt} = -u_i(t|\mathbf{W}, x') + I_i(t|\mathbf{W}, x') - \tau_m r_i(\mathbf{W}, x') V_{th}^i(t|\mathbf{W}, x') \quad (30)$$

Subtracting (26) from (30) and employing (29), denoting

$$\Delta I_i(t|\mathbf{W}, x') \triangleq I_i(t|\mathbf{W}, x') - I_i^*(t|\mathbf{W}^*, \mathcal{D}) \quad (31)$$

we derive the 1st-order dynamic of $e_i(t|\mathbf{W}, x')$

$$\tau_m \frac{de_i(t|\mathbf{W}, x')}{dt} = -e_i(t|\mathbf{W}, x') + \Delta I_i(t|\mathbf{W}, x') - \tau_m [r_i(\mathbf{W}, x') V_{th}^i(t|\mathbf{W}, x') - r_i^*(\mathbf{W}^*, \mathcal{D}) V_{th}] \quad (32)$$

Differentiating (32) with respect to time and utilizing the threshold dynamics from (29), we obtain:

$$\tau_m \frac{d^2 e_i(t|\mathbf{W}, x')}{dt^2} = -\frac{de_i(t|\mathbf{W}, x')}{dt} + \frac{d\Delta I_i(t|\mathbf{W}, x')}{dt} - \tau_m \theta_i r_i(\mathbf{W}, x') e_i(t|\mathbf{W}, x') \quad (33)$$

For succinctness, we will omit dependencies on \mathbf{W} and x' , resulting in TA-LIF dynamics in the main text (25):

$$\tau_m \frac{d^2 e_i(t)}{dt^2} + \frac{de_i(t)}{dt} + r_i \tau_m \theta_i e_i(t) = \frac{d\Delta I_i(t)}{dt} \quad (34)$$

For the standard LIF neurons where $\theta_i \rightarrow 0$, the equation simplifies to:

$$\tau_m \frac{d^2 e_i(t)}{dt^2} + \frac{de_i(t)}{dt} = \frac{d\Delta I_i(t)}{dt} \quad (35)$$

B Dynamic Stability Analysis

In this section, we analyze the stability of (34) and (35) to explore the influence of our dynamic threshold mechanism on the noise suppression ability of TA-LIF neuron.

B.1 BIBO Stability of Equation (34)

Characteristic Equation: We first show the BIBO (Bounded Input, Bounded Output) stability [45] of TA-LIF neurons based on (34). The characteristic equation of (34) of non-silent ($r_i > 0$) and non-degenerating ($\tau_m, \theta_i > 0$) TA-LIF neurons are:

$$\tau_m s^2 + s + r_i \tau_m \theta_i = 0 \quad (36)$$

and its roots are

$$s_{1,2} = \frac{-1 \pm \sqrt{\Delta}}{2\tau_m}, \quad \Delta = 1 - 4r_i \tau_m^2 \theta_i \quad (37)$$

- For $\Delta > 0$: Both roots $s_{1,2}$ are real and negative.
- For $\Delta = 0$: There's a single negative real root.
- For $\Delta < 0$: Both roots are complex with negative real parts.

For a second-order system to be BIBO, the roots of its characteristic equation must be a negative real or have a negative parts, which is clearly the case for the TA-LIF model under the above three situations, affirming the BIBO stability of (34). The BIBO stability signifies that with the bounded driving input to system (34), the deviation of the TA-LIF neuron's membrane potential from its targeted NDS is also bounded, demonstrating the well control of the growth of error $e_i(t)$.

B.2 Stability of Equation (34) Under White Noise

To elucidate the dynamic characteristics of TA-LIF further, we adopt the prevalent method [1, 9, 21, 49], approximating $\Delta I(t)$ with a Wiener process. This approximation effectively represents small, independent, and random perturbations. Hence, the driving force in equation (34) $\frac{d\Delta I_i(t)}{dt}$ can be modeled by a Gaussian white noise $F(t)$, leading to the well-established Langevin equation in stochastic differential equations theory [27, 61, 50]:

$$\frac{d^2 e_i(t)}{dt^2} + \frac{1}{\tau_m} \frac{de_i(t)}{dt} + r_i \theta_i e_i(t) = F(t) \quad (38)$$

Denoting $\langle \cdot \rangle$ as averaging over time, $F(t)$ is a Gaussian white noise with variance σ^2 which satisfies:

$$\begin{cases} \langle F(t) \rangle & = 0, \\ \langle F(t_1) F(t_2) \rangle & = \sigma^2 \delta(t_1 - t_2), \\ \langle F(t_1) F(t_2) \cdots F(t_{2n+1}) \rangle & = 0, \\ \langle F(t_1) F(t_2) \cdots F(t_{2n}) \rangle & = \sum_{\text{all pairs}} \langle F(t_i) F(t_j) \rangle \cdot \langle F(t_k) F(t_l) \rangle \cdots \end{cases} \quad (39)$$

where the sum has to be taken over all the different ways in which one can divide the $2n$ time points $t_1 \cdots t_{2n}$ into n pairs. Under this assumption (39), the solution of the Langevin equation(38) is [60, 62]:

$$\langle [\Delta e_i(t)]^2 \rangle = \frac{\tau_m \sigma^2}{2r_i \theta_i} \left[1 - e^{\frac{-t}{2\tau_m}} \left(\cos(\omega_1 t) + \frac{\sin(\omega_1 t)}{2\omega_1 \tau_m} \right) \right] = O(\sigma^2) \quad (40)$$

where $\Delta e_i(t) = e_i(t) - \langle e_i(t) \rangle$ and $\omega_1 = \sqrt{r_i \theta_i - \frac{1}{4\tau_m^2}}$. While under the same assumptions (39), equation (35) yields:

$$\langle [\Delta e_i(t)]^2 \rangle = \frac{\tau_m^2 \sigma^2}{2} \left(t - \tau_m + \tau_m e^{-t/\tau_m} \right) = O(\sigma^2 t) \quad (41)$$

Obviously, gaussian white noise with zero mean (39) leads $\langle e_i(t) \rangle = 0$, $\langle [\Delta e_i(t)]^2 \rangle = \langle e_i^2(t) \rangle$. Hence,

$$\frac{d\Delta I(t)}{dt} \sim F(t) \implies \begin{cases} \langle e_i^2(t) \rangle_{LIF} = O(\sigma^2 t) \\ \langle e_i^2(t) \rangle_{TA-LIF} = O(\sigma^2) \end{cases} \quad (42)$$

Significantly, the mean square error $\langle e_i^2(t) \rangle_{TA-LIF}$ of the TA-LIF neuron remains bounded to $O(\sigma^2)$ and doesn't increase over time. In contrast, under identical input perturbations, the mean square error $\langle e_i^2(t) \rangle_{LIF}$ of the LIF neuron may grow unbounded with time, highlighting its potential susceptibility to adversarial attacks.

C Experiment Setting Details

Our evaluation encompasses three benchmark datasets: FashionMNIST, SVHN, CIFAR10, and CIFAR100. For experimental setups, we deploy:

- LeNet (32C5-P-64C5-P-1024-10) for FashionMNIST.
- VGGs (32C3-32C3-P-64C3-P-128C3-128C3-128-10) for SVHN.
- VGGs (128C3-P-256C3-P-512C3-1024C3-512C3-1024-512-10) for CIFAR10.
- VGGs (128C3-P-256C3-P-512C3-1024C3-512C3-1024-1024-100) for CIFAR100.

Here, the notation 32C3 represents a convolutional layer with 32 filters of size 3×3 , and P stands for a pooling layer using 2×2 filters. For the CIFAR10 and CIFAR100 datasets, we incorporated Batch normalization layers and dropout mechanisms to mitigate overfitting and elevate the performance of the deep networks. In our experiments with FashionMNIST, SVHN and CIFAR10, the output spike train of LIF neurons was retained to compute the kernel loss, as described in [68]. For CIFAR100, we directly employed softmax for performance.

For all HoSNN experiments, a preliminary training phase was carried out using an LIF SNN, sharing the same architecture, on the clean datasets to deduce the NDS. Hyperparameters for LIF and TA-LIF neurons included a simulation time $T = 5$, a Membrane Voltage Constant $\tau_m = 5$, and a Synapse Constant $\tau_s = 3$. For the TA-LIF results in the main text, we assigned θ_i initialization values of 5 for FashionMNIST, SVHN, CIFAR10 and 3 for CIFAR100. All neurons began with an initial threshold of 1. The step function was approximated using $\sigma(x) = \frac{1}{1+e^{-5x}}$, where $x = u(t) - V_{th}(t)$ and the BPTT learning algorithm was employed. For TA-ALIF neurons, the learning rate for θ_i was set at 1/10 of the rate designated for weights, ensuring hyperparameter stability during training. We also constrained θ_i to remain non-negative during optimization, ensuring a possible transition from TA-LIF to LIF. For the generation of all gradient-based adversarial attacks, we assume that the attacker can know all $V_{th}(t)$ and use it in the gradient, even if it is generated dynamically and is not stored as network parameters. During training we use $V_{th}(t) = V_{th}(0)$. We utilized the Adam optimizer with hyperparameters betas set to (0.9, 0.999), and the $lr = 5 \times 10^{-4}$ with cosine annealing learning rate scheduler ($T = \text{epochs}$). We set batch size to 64 and trained for 200 epochs. All images were transformed into currents to serve as network input. Our code is adapted from [68]. The experiment used four NVIDIA A100 GPUs. For cifar10 and cifar100, it took up to about 48 hours for adversarial training.

Regarding adversarial attack, we use an array of attack strategies, including FGSM, RFGSM, PGD, and BIM. For both CIFAR10 and CIFAR100, we allocated an attack budget with $\epsilon = 8/255$. For iterative schemes like PGD, we set $\alpha = \epsilon/3$ and $steps = 7$, aligning with the recommendations in [15]. For the adversarial training phase, FGSM training was used with ϵ values of 2/255 for CIFAR10 (as per [15]) and 4/255 for CIFAR100, following [29].

D Checklist for Gradient obfuscation

Obfuscated gradients are a type of gradient masking that lead to a false sense of security when defending against adversarial examples [4, 10]. Here we perform sanity checks including three obfuscated types and checklist as per [4].

First we examine three types of obfuscated gradients. Specifically, we use the same surrogate to train HoSNN from scratch and deliver attacks, decent clean accuracy and smooth training process indicate that it's not **Shattered Gradient** with nonexistent or incorrect value. As our defense doesn't introduce any random factors, **Stochastic Gradient** is not applicable. Our method also doesn't include any multiple iterations of neural network evaluation, so **Vanishing/Exploding Gradient** are also not applicable.

Items to identify gradient obfuscation	HoSNN
(1) Single-step attack performs better compared to iterative attacks	✓
(2) Black-box attacks perform better compared to white-box attacks	✓
(3) Increasing perturbation bound can't increase attack strength	✓
(4) Unbounded attacks can't reach $\sim 100\%$ success	✓
(5) Adversarial example can be found through random sampling	✓

Then let's check the item in checklist one by one.

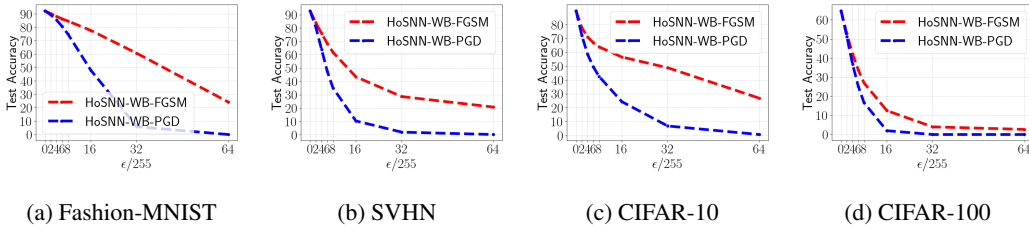


Figure 7: For Test (1). Performance of HoSNN under white-box FGSM and PGD attack.

For **Test (1): Single-step attack performs better compared to iterative attacks**, we plot the curves of white-box FGSM and PGD attacks on four datasets in Figure 7, with attack budgets ϵ from 0 to 64/255 to ensure that the network can be completely fooled. The red curve is the accuracy under FGSM, while the blue curve is PGD. From the Figure 7 we can confirm that all iterative attacks are much stronger than single-step attack.

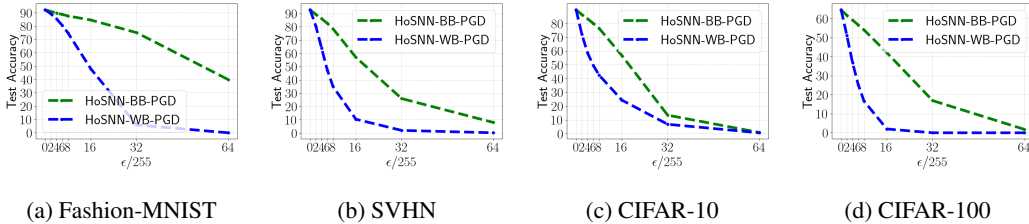


Figure 8: For Test (2). Performance of HoSNN under white-box and black-box and PGD attack.

For **Test (2): Black-box attacks performs better compared to white-box attacks**, we plot the curves of white-box and black-box PGD attacks on four datasets in Figure 8, with attack budgets ϵ from 0 to 64/255 to ensure that the network can be completely fooled. The green curve is the accuracy under black-box PGD attack, while the blue curve is under white-box. From the Figure 8 we can confirm that all white-box attacks are much stronger than black-box.

For **Test (3) & (4): Increasing perturbation bound can't increase attack strength & Unbounded attacks can't reach $\sim 100\%$ success**, we plot the curves of white-box and black-box PGD attacks on four datasets in Figure 9, with attack budgets ϵ from 0 to 64/255 to ensure that the network can be completely fooled. The blue curve is HoSNN's accuracy under white-box PGD attack, while the yellow curve is SNN's baseline. From the Figure 9 we can confirm that as perturbation bound increasing HoSNN's accuracy is decreasing and all unbounded attacks reach $\sim 100\%$ success.

For **Test (5) Adversarial example can be found through random sampling**, since all gradient-based attacks work, there is no need to use random sampling methods. Therefore Test (5) passed obviously. All five gradient obfuscation test passed.

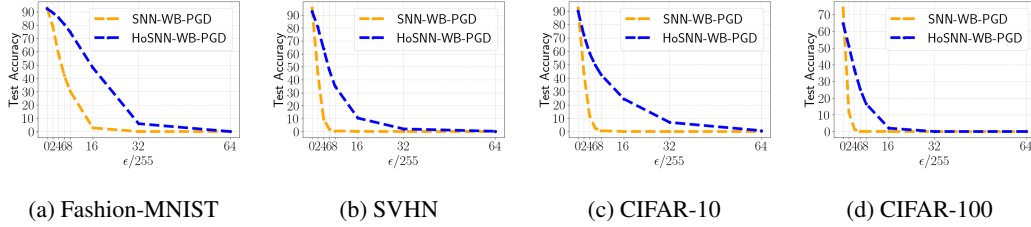


Figure 9: For Test(3) and (4). Performance of HoSNN under larger white-box PGD attack.

E Supplementary Data

Table 2: HoSNN accuracy data for Test1. We compared the performance under white-box FGSM and PGD attack. Our data shows that single-step attacks are strictly weaker than multi-step attacks.

Dataset	Method	$\epsilon = 0$	2	4	6	8	16	32	64
FMNIST	WB-FGSM	92.31	90.26	88.16	86.25	84.70	77.70	60.70	24.27
	WB-PGD	92.31	89.34	85.44	80.61	74.91	47.93	5.87	0.00
SVHN	WB-FGSM	92.84	83.96	75.85	68.45	61.78	43.45	28.64	20.79
	WB-PGD	92.84	80.53	63.98	47.56	35.06	10.40	2.00	0.21
CIFAR-10	WB-FGSM	90.00	77.84	71.14	67.05	63.98	56.66	48.92	26.93
	WB-PGD	90.00	72.24	58.66	49.65	42.63	24.38	6.82	0.65
CIFAR-100	WB-FGSM	64.63	52.78	42.12	33.79	26.97	12.47	4.01	2.68
	WB-PGD	64.64	51.20	36.82	25.23	16.65	1.99	0.00	0.00

Table 3: HoSNN accuracy data for Test2. We compared the performance under white-box PGD and black-box PGD attack. Our data shows that black-box attacks are strictly weaker than white-box attacks.

Dataset	Method	$\epsilon = 0$	2	4	6	8	16	32	64
FMNIST	BB-PGD	92.31	91.05	89.81	88.85	87.67	84.61	75.12	39.93
	WB-PGD	92.31	89.34	85.44	80.61	74.91	47.93	5.87	0.00
SVHN	BB-PGD	92.84	89.31	86.10	82.68	78.49	57.02	25.96	8.02
	WB-PGD	92.84	80.53	63.98	47.56	35.06	10.40	2.00	0.21
CIFAR-10	BB-PGD	90.00	86.55	83.46	80.11	76.61	56.77	13.43	0.92
	WB-PGD	90.00	72.24	58.66	49.65	42.63	24.38	6.82	0.65
CIFAR-100	BB-PGD	64.64	61.68	59.22	56.67	54.06	42.08	16.90	1.82
	WB-PGD	64.64	51.20	36.82	25.23	16.65	1.99	0.00	0.00

Table 4: HoSNN accuracy data for Test3. We showed the performance of SNN and HoSNN under white-box PGD attack. Our data shows that increasing perturbation bound can increase attack strength and the accuracy can drop to 0 as the attack becomes stronger.

Dataset	Method	$\epsilon = 0$	2	4	6	8	16	32	64
FMNIST	SNN-WB-PGD	92.92	78.87	58.03	42.27	30.54	2.71	0.00	0.00
	HoSNN-WB-PGD	92.31	89.34	85.44	80.61	74.91	47.93	5.87	0.00
SVHN	SNN-WB-PGD	95.51	44.78	9.66	1.83	0.44	0.10	0.02	0.01
	HoSNN-WB-PGD	92.84	80.53	63.98	47.56	35.06	10.40	2.00	0.21
CIFAR-10	SNN-WB-PGD	92.47	44.00	11.73	2.46	0.56	0.01	0.00	0.00
	HoSNN-WB-PGD	90.00	72.24	58.66	49.65	42.63	24.38	6.82	0.65
CIFAR-100	SNN-WB-PGD	74.00	11.62	1.29	0.13	0.04	0.00	0.00	0.00
	HoSNN-WB-PGD	64.64	51.20	36.82	25.23	16.65	1.99	0.00	0.00